Sensing and Bio-Sensing Research 7 (2016) 31–37

Contents lists available at ScienceDirect

Sensing and Bio-Sensing Research

journal homepage: www.elsevier.com/locate/sbsr

Quantitative analysis of impact measurements using dynamic load cells

Brent J. Maranzano *, Bruno C. Hancock

Pfizer Global Research and Development, Groton, CT 06340, USA

ARTICLE INFO

Article history:
Received 17 March 2015
Accepted 9 November 2015

Keywords:
Young's modulus
Poisson's ratio
Dynamic load cell

ABSTRACT

A mathematical model is used to estimate material properties from a short duration transient impact force measured by dropping spheres onto rectangular coupons fixed to a dynamic load cell. The contact stress between the dynamic load cell surface and the projectile are modeled using Hertzian contact mechanics. Due to the short impact time relative to the load cell dynamics, an additional Kelvin–Voigt element is included in the model to account for the finite response time of the piezoelectric crystal. Calculations with and without the Kelvin–Voigt element are compared to experimental data collected from combinations of polymeric spheres and polymeric and metallic surfaces. The results illustrate that the inclusion of the Kelvin–Voigt element qualitatively captures the post impact resonance and non-linear behavior of the load cell signal and quantitatively improves the estimation of the Young's elastic modulus and Poisson's ratio. Mathematically, the additional KV element couples one additional differential equation to the Hertzian spring-dashpot equation. The model can be numerically integrated in seconds using standard numerical techniques allowing for its use as a rapid technique for the estimation of material properties.

1. Introduction

Load cells are transducers that produce an electrical signal when subjected to a force and are commonly used in laboratory instruments to measure static and dynamic forces. Of particular interest in this paper are load cells that utilize a piezoelectric material to generate the electrical signal. Due to the rigidity of many piezoelectric materials, piezoelectric type load cells provide rapid response to dynamically varying forces, and have been used in numerous studies to quickly characterize, or sort materials from impact experiments [1–4].

For many experiments, empirical analysis of dynamic load cell (DLC) measurement data is sufficient for qualitative material characterization. However, the transient impact force data measured by a DLC can be used to quantitatively estimate material properties given a model for the impact collision, and a constitutive equation for the materials properties [5,6]. Due to the stiffness of the common load cell strike surface (typically a steel alloy) relative to the test material, the deformation of the load cell can often be neglected when modeling the impact collision. Moreover, the response time of dynamic load cells is often sufficiently fast that the output signal can be assumed to be directly proportional to the instantaneous contact force. Consequently, the impact dynamics can be approximated as a collision between the test material and an elastic half space with an infinite modulus. This approximation, however, may not be valid for materials with a high modulus, or for collisions with very short duration.

The minimum impact duration (maximum frequency) accurately measured by a dynamic load cell is due to the small but finite deflection of the piezoelectric material necessary to generate the electric field. For measurements that occur at time scales substantially longer than the natural resonant frequency of the crystal, the crystal load can be approximated as quasi static. For a quasi static load, the crystal deformation and electrical signal are directly proportional to the normal force, and the crystal inertia can be ignored, as in the assumption of an elastic half space. However, for transient loads that have characteristic time scales comparable to the crystal resonance time scale, the inertia of the crystal may not be negligible, and could give rise to a non-linear response between the dynamic load and the output signal [6].

Ideally, the load cell used in an experiment should have a natural frequency that is substantially greater than the highest Fourier frequency being measured. However, due to limitations in real-life load cell designs, it may not be possible to utilize a load cell that fulfills the resonant frequency requirement. In such cases, it would be beneficial to have a model that incorporates the load cell dynamics into an impact model that can improve the measurement accuracy. The goal of this paper is to derive a model for the transient response of the piezoelectric crystal in a dynamic load cell, and compare experimental impact force measurements to predictions with and without explicit modeling of the crystal dynamics.

2. Material and methods

The impact measurement instrument consists of a custom built aluminum stand (MDC Associates) that holds a vacuum tube stationary

* Corresponding author.
E-mail addresses: Brent.Maranzano@pfizer.com (B.J. Maranzano), Bruno.Hancock@pfizer.com (B.C. Hancock).

http://dx.doi.org/10.1016/j.sbsr.2015.11.005

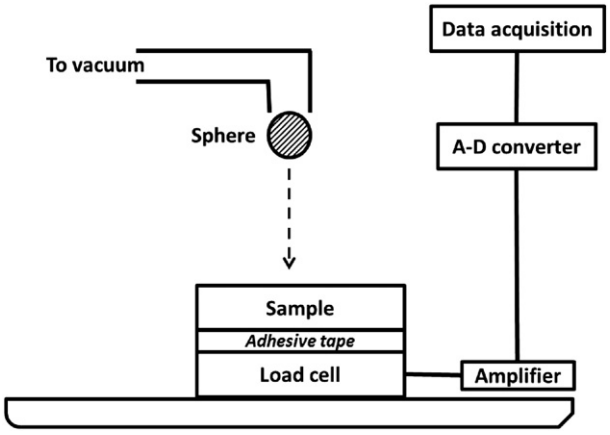

Fig. 1. Schematic of the impact measurement setup.

above a dynamic load cell (Omega DLC101-10) (see Fig. 1). The amplified (Omega ACC-PS3A) analog voltage of the load cell is digitized at a sampling rate of 1 MHz with an analog digital converter (Omega OMB-DAQ-3500) that is triggered and controlled by custom software [7,8].

Rectangular samples are attached to the load cell strike cap using double sided adhesive tape. It is necessary that the compact be rigidly secured to the load cell strike cap, such that entire impact force on the compact surface is transmitted to the load cell. Next, a sphere is attached to the end of the vacuum tube at a set height above the compact. Disengaging the vacuum releases the sphere to impact the surface of the compact. The impact produces a transient voltage signal, which is digitized and stored onto a computer for subsequent analysis. The mechanical properties of the compact and sphere are extracted from the experimental data by iteratively adjusting the compact Young's modulus of elasticity, Poisson's ratio and coefficient of restitution to fit the theory.

The load cell parameters are estimated by dropping spheres of known mechanical properties (Table 1) onto surfaces with known mechanical properties (Table 2) and fitting the transient voltage signal to the theory. The coefficient of restitution for each sphere and surface pair is determined by measuring the sphere rebound height from slow playback of videos recorded during the impact.

Table 1
Sphere properties.

Material	Property	Value
Steel	Radius	0.299
	Modulus (GPa)	194
	Poisson's ratio	0.33
	Mass (g)	.8780
Acetal resin	Radius	0.476
	Modulus (GPa)	3.0–3.3
	Poisson's ratio	0.35
	Mass (g)	0.6116
Polypropylene	Radius	0.476
	Modulus (GPa)	2.8–3.5
	Poisson's ratio	0.38
	Mass (g)	0.4024
HDPE	Radius	0.476
	Modulus (GPa)	1.08
	Poisson's ratio	0.35
	Mass (g)	0.4232
PTFE	Radius	0.476
	Modulus (GPa)	0.5
	Poisson's ratio	0.46
	Mass (g)	0.9692
Neoprene	Radius	0.318
	Modulus (GPa	0.082
	Poisson's ratio	0.499
	Mass (g)	0.1981

Table 2
Properties of rectangular samples.

Material	Property	Range
Aluminum	Modulus (GPa)	69
	Poisson's ratio	0.33
PVC	Modulus (GPa)	2.5–4.0
	Poisson's ratio	0.38–4.1
Polycarbonate	Modulus (GPa)	2.0–2.4
	Poisson's ratio	0.37

3. Theory

Following the analysis by Maranzano et al. [6], the trajectory of a sphere during impact with a load cell is described by Newton's second law of motion (Eq. (1)), where the forces exerted on the sphere include, the gravitational force, F_{grav}, an elastic deformation force, F_{el}, and a dissipative deformation force, F_{dis}.

$$\frac{d}{dt}(mv)_{sph} = F_{el}(\delta) + F_{dis}\left(\dot{\delta}\right) - F_{grav} \tag{1}$$

Here, m is the sphere mass and v is sphere velocity. The Hertzian spring-dashpot model provides expressions for the elastic force as a function of the deformation, δ (Eq. (2)), and the dissipative force as a function of the deformation rate, $\dot{\delta}$. (Eq. (3)).

$$F_{el} = K\delta^{32} \tag{2}$$

$$F_{dis} = \alpha(\epsilon)\sqrt{mK}\delta^{1/4}\dot{\delta} \tag{3}$$

The material constant, K, in Eqs. (2) and (3), is related to the modulus of the compact, E_1, the modulus of the planar surface, E_2, the Poisson ratio of the compact, ν_1, and the Poisson ratio of the planar surface, ν_2, by:

$$K = \frac{\frac{4\sqrt{R}}{3}}{\frac{1-\nu_1^2}{E_1} + \frac{1-\nu_2^2}{E_2}} \tag{4}$$

The expression for a dissipative force constant, α, in Eq. (3) is a function of the coefficient of restitution, ϵ 5[9,10].

$$\alpha(\epsilon) = \frac{-\sqrt{5}\ln\epsilon}{\sqrt{\ln^2\epsilon + \pi^2}} \tag{5}$$

And the coefficient of restitution is defined in terms of compact deformation as:

$$\epsilon \equiv -\frac{\dot{\delta}(\tau)}{\dot{\delta}(0)} \tag{6}$$

where, τ is defined as the duration of the impact, which begins at time zero.

Experimentally the signal generated by the load cell is caused by the deflection of an internal piezoelectric crystal, which generates an electric field when deformed. Due to the rigidity of the crystal and the load cell design, the crystal deflection is usually very small relative to the deformation of the impacting body. Furthermore the dynamics of the crystal (which is proportional to the square-root of the crystal stiffness divided by the crystal mass) are typically much faster than the impact transients. Thus, for many applications the crystal deflection is in a quasistatic equilibrium with the instantaneous load cell contact forces.

For this assumption, the load cell signal voltage is directly proportional to the instantaneous elastic deformation force.

$$V_{\text{loadcell}} \propto F_{\text{el}}(\delta) \tag{7}$$

Thus, provided the material properties for the impact sphere and surface, Eqs. (1) through (6) can be used to solve for the theoretical elastic force, or conversely, an experimentally measured transient load cell force can be used to estimate the modulus and Poisson's ratio of the impacting sphere and surface. In this paper this model will be referred to as the Hertz spring-dashpot (HSD) model.

For impact collisions with transients of the same time scale as the load cell dynamics, the crystal deflection may not be in a quasistatic equilibrium with the net contact forces as per Eq. (7). Therefore an alternative relationship is required to relate the theoretical impact dynamics to the load cell signal. One possibility to account for the crystal dynamics is to model the crystal as a Kelvin–Voigt element, which consists of a spring and a dash-pot in parallel. For this case, the elastic contact force is coupled to the crystal deflection through a second invocation of Newtons' second law.

$$\frac{d}{dt}(mv)_{\text{crystal}} = -F_{\text{el}}(\delta) + F_{\text{sp}}(\Delta) - F_{\text{dash}}\left(\dot{\Delta}\right) \tag{8}$$

Here, F_{sp} represents the restoration force of the crystal to equilibrium as a function of the deflection Δ, F_{dash} is the dissipative force opposing the crystal movement as a function of the deflection rate $\dot{\Delta}$, and F_{el} is the Hertz contact elastic force.

To minimize the number of adjustable parameters, the spring force, F_{sp}, and dash-pot force, F_{dash}, are assumed to be proportionally related to the crystal deflection, and rate of crystal deflection, respectively.

$$F_{\text{sp}} = k\Delta \tag{9}$$

and

$$F_{\text{dash}} = \mu\dot{\Delta} \tag{10}$$

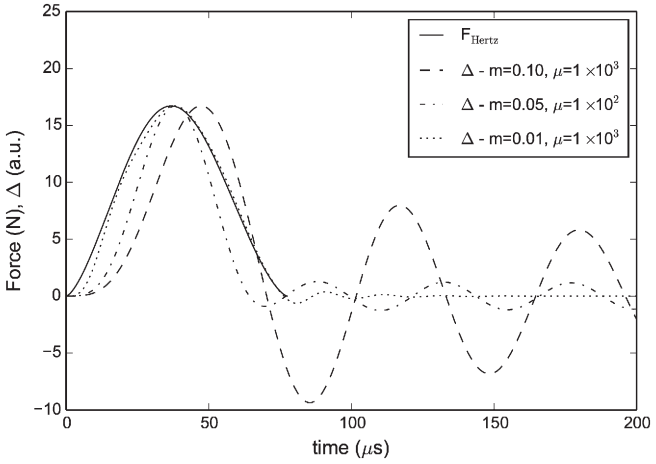

Fig. 3. Comparison of the theoretical Hertzian contact force calculated (solid line), to scaled load cell crystal deflections, Δ, calculated from the KV model for varying load cell parameters, and identical material properties as given in Fig. 2. Here, m is the crystal mass, and μ is the dissipative constant. Note that the crystal deflection has been scaled such that the maximum in all curves are identical.

Finally, the load cell signal is postulated to be proportional to the crystal deflection Δ.

$$V_{\text{load cell}} \propto \Delta \tag{11}$$

Eqs. (8)–(10) augment Eq. (7) to relate the elastic contact force to the load cell signal for measurements that have transient dynamics near the same time scale as the load cell dynamics, and will be referred to in this paper as the Kelvin–Voigt (KV) model.

4. Results

Fig. 2 compares the Hertzian contact force, surface deformation, and crystal deflection for the Kelvin–Voigt model. The finite inertia of the crystal causes several deviations between the crystal deflection and the contact force. First, the crystal deflection is delayed by approximately 10 μs relative to the contact force. Furthermore, due to the delayed

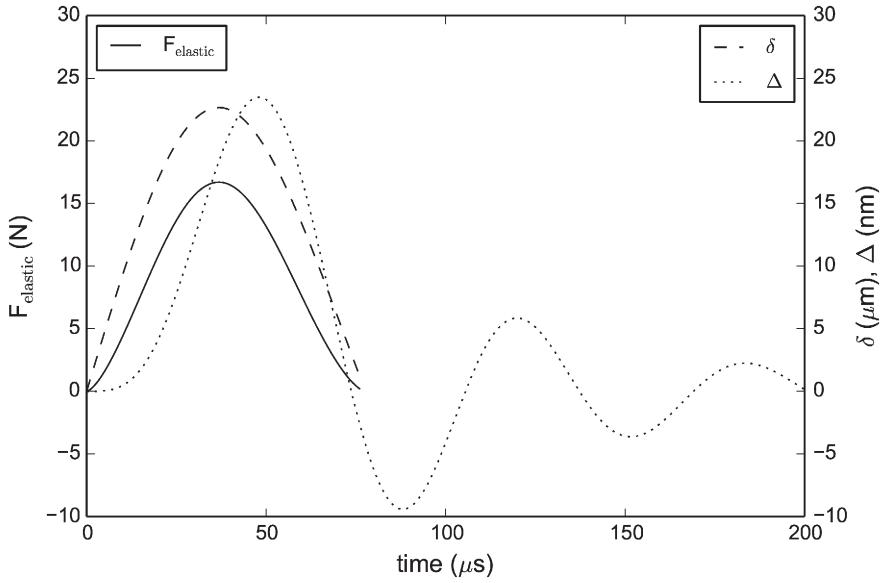

Fig. 2. Theoretical Hertzian contact force, surface deformation, and crystal deflection obtained by numerically solving the Kelvin–Voigt model for a 0.407 g sphere of radius 0.476 cm with modulus and Poisson's ratio of 3.0 GPa and 0.33, respectively, dropped 4.7 cm onto a surface with modulus and Poisson's ratio of 3.0 GPa and 0.33, respectively. The values for the mass, stiffness, and damping of the crystal used are: 100 g, 1.0 GN/m, and 3.0 kN s/m.

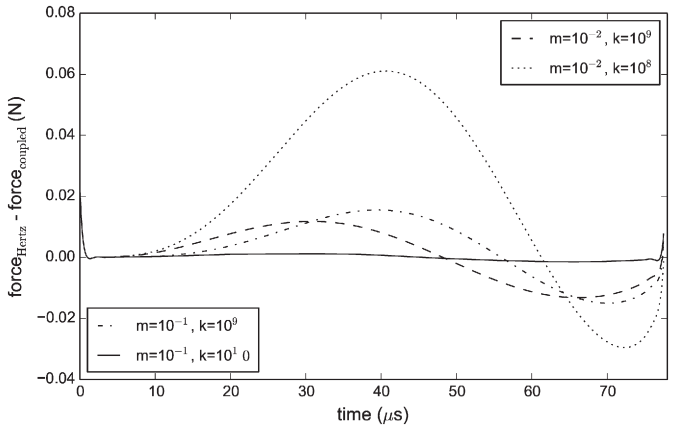

Fig. 4. Difference between the theoretical Hertzian contact force calculated from the HSD model the theoretical Hertzian contact force calculated from Kelvin–Voigt model for varying mass, m, and stiffness, k, of the load cell crystal.

response of the crystal, the crystal deflection continues increasing after the contact force reaches a maximum, which leads to an asymmetry in the crystal trajectory. Lastly, the finite inertia of the crystal causes the crystal to oscillate around its unloaded equilibrium position for several hundred microseconds after the impact.

Quantitatively, the delay in crystal response and the period of the oscillation is proportional to the square root of the crystal mass divided by the crystal stiffness, and the rate of decay of the post impact crystal oscillation is proportional to the crystal damping factor. Fig. 3 compares the theoretical Hertzian contact force with the theoretical crystal deflection from the KV model for a set of crystal mass and crystal damping factors and for constant set of sphere and surface properties. The calculated signals have been scaled to have the same peak amplitude to facilitate comparison with the theoretical Hertzian contact force. The plot demonstrates the response time decreases as the crystal mass decreases (for a constant crystal stiffness), and that the oscillation decreases with increasing damping. Load cells are designed to minimize the response delay and oscillation, but due to physical limitations, cannot eliminate them.

While the crystal properties determine the load cell dynamics, the crystal properties do not substantially influence the physical dynamics between the load cell surface and the projectile. The negligible contribution of the crystal deflection to the impact dynamics is suggested by Fig. 2, which demonstrates that the sphere deformation, δ, is nearly three orders of magnitude greater than the crystal deflection, Δ. Fig. 4 further confirms that the dynamic contact force is not substantially influenced by the crystal properties, by comparing the difference in the Hertzian contact force calculated from the HSD model to the Hertzian contact force calculated from the KV model. For this range of crystal mass and crystal stiffness, the maximum difference in the theoretical Hertzian

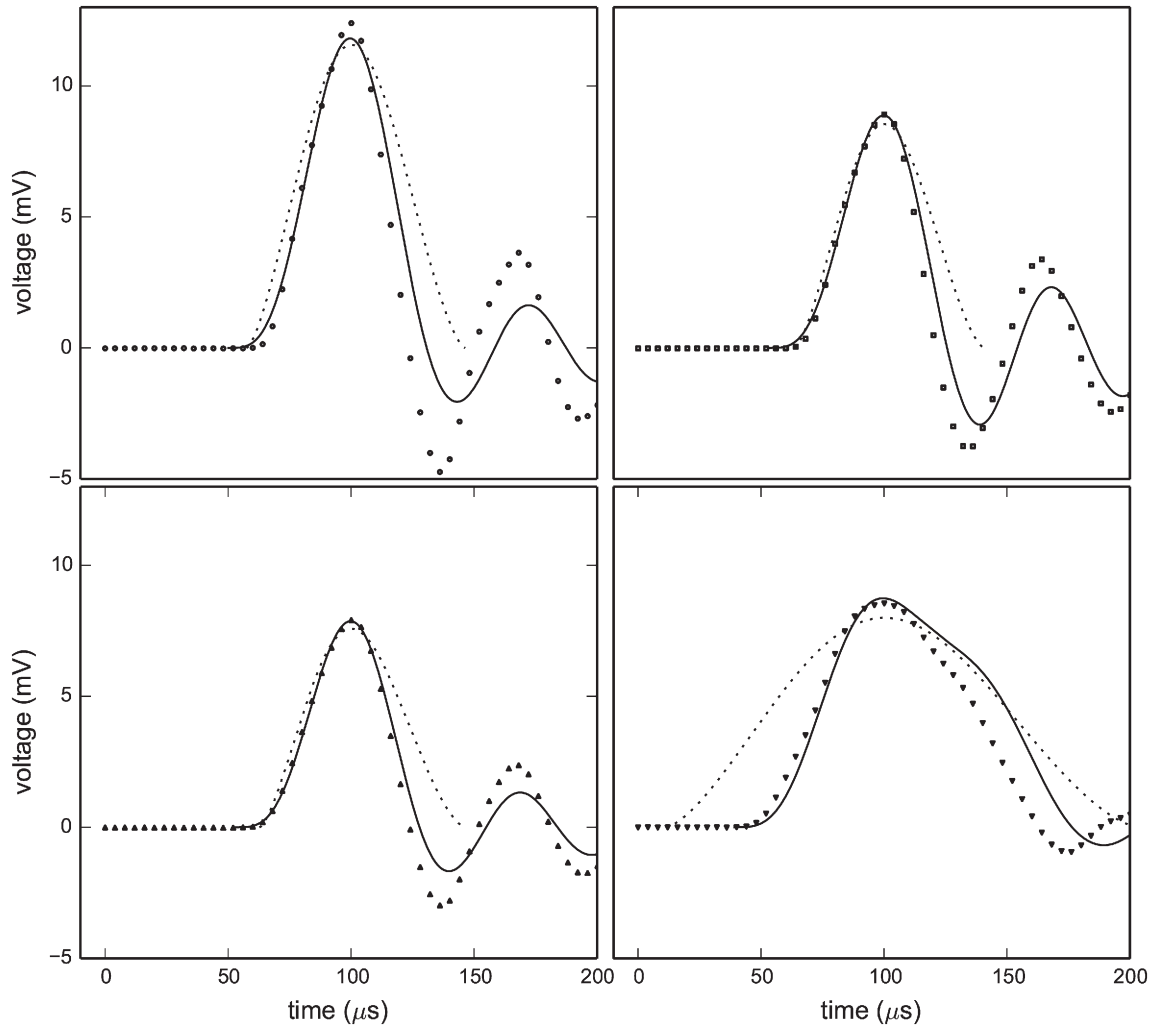

Fig. 5. Measured load cell voltage (filled circles), predicted voltage assuming the voltage is proportional to the elastic contact force as given in Eq. (7) (dotted line), and the predicted voltage assuming the voltage is proportional to the quartz crystal deformation as given in Eq. (11) (solid line) for the impact of spheres made of acetal resin (top left), polypropylene (top right), HDPE (bottom left), and PTFE (bottom right) against a polycarbonate surface.

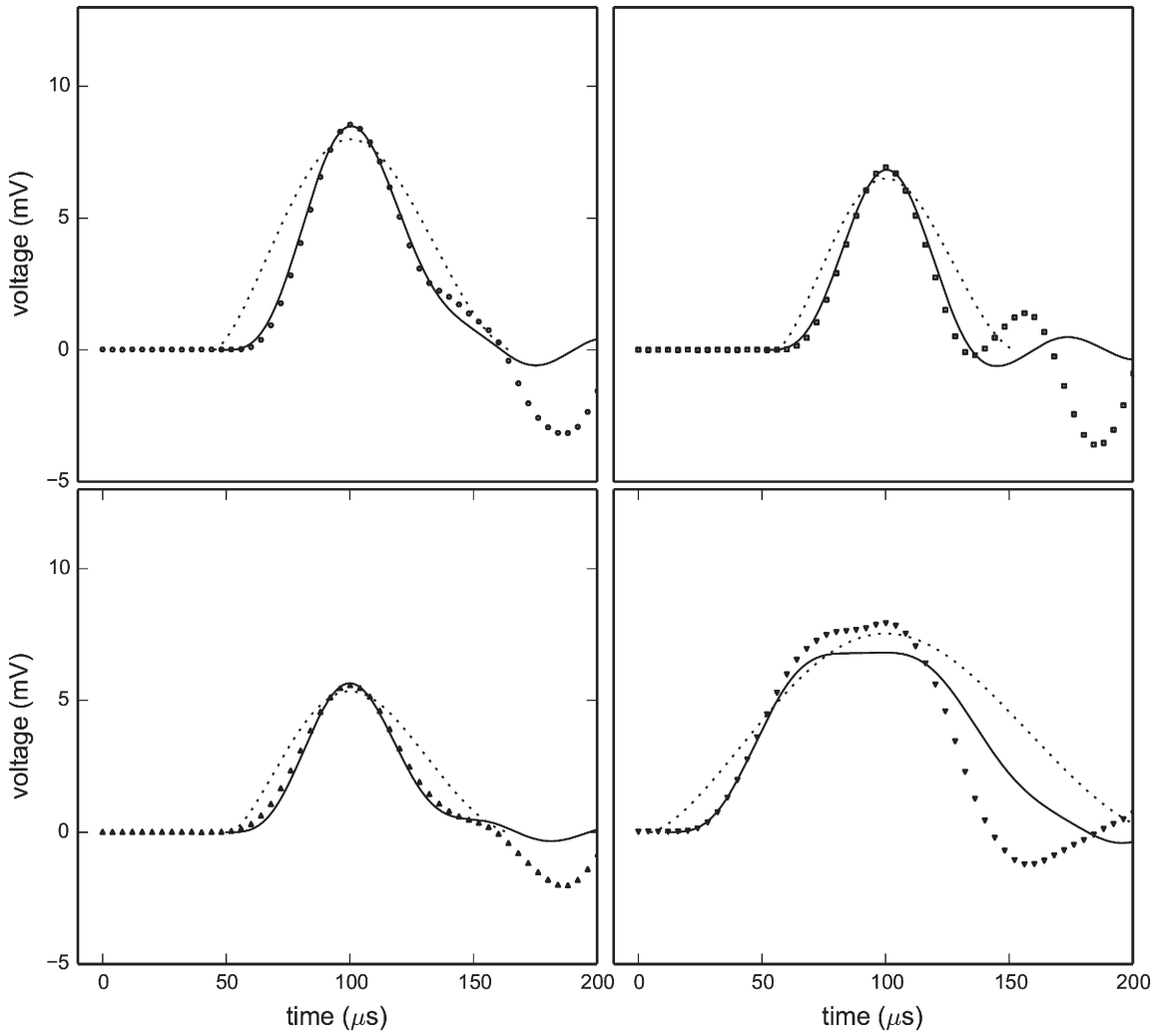

Fig. 6. Measured load cell voltage (filled circles), predicted voltage assuming the voltage is proportional to the elastic contact force as given in Eq. (7) (dotted line), and the predicted voltage assuming the voltage is proportional to the quartz crystal deformation as given in Eq. (11) (solid line) for the impact of spheres made of acetal resin (top left), polypropylene (top right), HDPE (bottom left), and PTFE (bottom right) against a PTFE surface.

contact forces is less than 0.1 N, which is less than a 1% difference. Consequently, the sphere-surface impact dynamics are essentially insensitive to the particular design of the load cell.

To estimate material properties from load cell impact measurements, the relationship between the contact force and load cell signal must be defined. For the HSD model only a single calibration parameter is required, which can be estimated by applying static weights to the load cell. Conversely, for the KV model the proportionality constant, as well as the crystal model parameters: crystal mass ($m_{crystal}$), crystal stiffness (k), and crystal damping (μ), can only be determined from dynamic measurements. One option to estimate these parameters is to fit the measured dynamic impact force for material of known properties using the crystal properties as adjustable fit parameters as demonstrated in Figs. 5 and 6.

Table 3
Mass (Eq. (8)), stiffness (Eq. (9)), damping coefficient (Eq. (10)), and calibration constant (Eq. (11)) of the crystal determined from fitting impact measurements of materials with known mechanical properties to theory.

Parameter	Mean	std
Eq. (7)		
Calibration (mN/mV)	1.78	0.09
R^2	0.70	0.18
Eqs. (8)–(11)		
Calibration (nm/mV)	0.0056	0.0002
Crystal mass (g)	35.4	3.1
Crystal stiffness (GN/m)	0.416	0.042
Crystal damping (kN s/m)	0.56	0.02
R^2	0.93	0.08

Fig. 5 compares the measured load cell signal, the theoretical signal predicted by the HSD model and the theoretical signal predicted by the KV model for experiments using four a set of spheres (acetal resin, polypropylene, HDPE, and PTFE) against a polycarbonate surface. The theoretical signals are calculated using model parameters determined by minimizing the residual errors between the measured signal and the theory. The plots clearly demonstrate that the KV model qualitatively captures the oscillation of the signal due to the post impact crystal vibration, whereas the HSD model cannot capture the oscillation as the model assumes the load cell behaves as an elastic half-space. The KV model also better models the transient response during impact (the first peak), such as the smoother initial increase and the asymmetry in the contact peak, which are directly attributable to the inertia of the crystal.

For the more massive, and lower modulus PTFE sphere, the impact duration appears to exceed the natural oscillation time of the crystal, which leads to an apparent flattening and broadening of the impact peak. The cause for the broadening is likely due to the crystal making making a second oscillation during the physical contact, where the

deflection of the crystal is quite large when the sphere is no longer in contact with the load cell surface.

The superposition of the second crystal oscillation during physical contact between the sphere and surface is more pronounced for lower modulus surface, such as PTFE as demonstrated in Fig. 6. For example, the impact of a polypropylene sphere against the PTFE surface, the second crystal oscillation peak is very evident at around 160 μs, which also is approximately the time that the sphere rebounds off of the surface according to the HSD theory. For the case of a PTFE sphere and a PTFE surface, the crystal appears to nearly complete the second oscillation before the sphere leaves the surface, which creates a very broad, but nearly symmetric transient signal.

The estimated HSD and KV model parameters obtained by fitting the measured signals are listed in Table 3. The average residual error of the fits is greater for the HSD model compared to the KV model. Moreover, the residual error of the fits for both models typically increases as the average modulus of the surface and sphere decreases. It is interesting to note that the regression values of the crystal parameters appear physically plausible based on literature for quartz dynamic load cells.

Using the mean values for the model parameters, the modulus and Poisson's ratio for a series of sphere and surface combinations is estimated from the experimental data, and are listed in Tables 4 and 5, for the HSD and KV models, respectively. Comparing the predicted Young's elastic modulus in Tables 5, and 4, with the literature values in Tables 1 and 2 it is evident that the Young's elastic modulus predicted by the KV model is more accurate than the HSD model. Moreover, the R^2 correlation coefficient between measurement and theory, is much greater for the HSD model (0.48) compared to the KV model (0.86).

The KV model also results in less variation in the prediction of the sphere modulus for a given surface compared to the HSD model. For example, the predicted modulus for the acetal spheres against the four surfaces ranges from 4.18 GPa to 6.85 GPa using the HSD model, and from 3.16 GPa to 3.91 GPa for the KV model. Similarly, the KV model has less prediction variability than the HSD model for a particular surface using different spheres.

Table 4
Modulus of surface, E_p and modulus of sphere, E_s determined by fitting impact measurement data to Eq. (7) using the dynamic load cell calibration listed in Table 3. The average residual of fit, R^2, is 0.48.

Surface	E_p	E_s
Steel		
Aluminum	67.80 ± 0.00	176.47 ± 0.00
Polycarbonate	3.65 ± 0.29	230.91 ± 30.39
Acetal		
Aluminum	72.38 ± 5.92	4.18 ± 0.08
PVC	4.20 ± 0.07	4.93 ± 0.41
Polycarbonate	4.37 ± 0.11	6.85 ± 1.21
PTFE	0.93 ± 0.14	4.56 ± 0.28
Polypropylene		
Aluminum	70.95 ± 1.96	2.57 ± 0.07
PVC	3.59 ± 0.59	2.90 ± 0.39
Polycarbonate	3.42 ± 0.64	3.19 ± 0.21
PTFE	0.90 ± 0.09	2.42 ± 0.21
HDPE		
Aluminum	68.09 ± 4.10	1.58 ± 0.06
PVC	4.07 ± 1.16	1.88 ± 0.12
Polycarbonate	2.87 ± 0.67	1.50 ± 0.22
PTFE	0.75 ± 0.03	1.14 ± 0.08
PTFE		
Aluminum	19.22 ± 9.51	0.97 ± 0.05
PVC	2.26 ± 0.90	0.92 ± 0.09
Polycarbonate	1.19 ± 0.39	1.01 ± 0.01
PTFE	0.62 ± 0.11	0.71 ± 0.24
Neoprene		
PTFE	0.21 ± 0.30	0.01 ± 0.02

Table 5
Modulus of surface, E_p and modulus of sphere, E_s determined by fitting impact measurement data to Eq. (8) using the dynamic load cell parameters listed in Table 3. The average residual of fit, R^2, is 0.86.

Surface	E_p	E_s
Steel		
Aluminum	54.59 ± 0.33	222.26 ± 1.01
Polycarbonate	2.73 ± 0.02	160.13 ± 4.10
Acetal		
Aluminum	69.43 ± 1.15	3.17 ± 0.04
PVC	2.60 ± 0.04	3.16 ± 0.05
Polycarbonate	2.35 ± 0.04	3.25 ± 0.04
PTFE	0.68 ± 0.02	3.91 ± 0.12
Polypropylene		
Aluminum	70.18 ± 1.35	1.77 ± 0.01
PVC	2.54 ± 0.08	1.94 ± 0.09
Polycarbonate	2.57 ± 0.06	2.05 ± 0.07
PTFE	0.78 ± 0.02	1.64 ± 0.15
HDPE		
Aluminum	65.45 ± 3.56	1.13 ± 0.06
PVC	2.69 ± 0.03	1.21 ± 0.03
Polycarbonate	2.87 ± 0.12	1.28 ± 0.05
PTFE	0.76 ± 0.04	1.22 ± 0.05
PTFE		
Aluminum	78.83 ± 2.93	0.73 ± 0.05
PVC	2.27 ± 0.10	0.59 ± 0.00
Polycarbonate	1.36 ± 0.04	0.32 ± 0.04
PTFE	0.63 ± 0.05	0.64 ± 0.01
Neoprene		
PTFE	0.59 ± 0.08	0.05 ± 0.01

5. Conclusions

A model for the dynamics of a piezoelectric crystal inside a dynamic load cell is presented and incorporated into a previously published model that assumes the load cell is an elastic half space for the transient impact force between a sphere and dynamic load cell. Theoretical predictions using both the half-space assumption and the deformable crystal are compared to experimental measurements using a series of spheres and a series of surfaces with a range of material properties. The augmented model that includes the crystal dynamics qualitatively captures the experimentally measured delayed response and ringing of the load cell, whereas the half-space model does not. Lastly, both the prediction accuracy and prediction precision are improved using the crystal model compared to the elastic half-space model. The augmented model improves the estimation of material properties from impact measurements using piezoelectric type dynamic load cells.

Appendix A. Supplementary data

Supplementary data to this article can be found online at http://dx.doi.org/10.1016/j.sbsr.2015.11.005.

References

[1] M. J. Delwiche, H. Arevalo, J. J. Mehlschau, Second generation impact force response fruit firmness sorter, Trans. Am. Soc. Agric. Biol. Eng.
[2] Y.-W. Wang, J. Wang, C. Yao, Q.-J. Lu, Firmness measurement of peach by impact force response, J. Zhejiang Univ. Sci. B 10 (12) (2009) 883–889.
[3] I. Kim, S.-B. Lee, Development of a novel microimpact-fategue tester and its application to impact reliability of lead-free solder joints, IEEE Components Packag. Manuf. Technol. Soc. 32 (3) (2009) 542–549.
[4] H. Ito, Y. Fujii, Evaluation of mechanical response of human palm to small impact force, Electron. Commun. Jpn. 92 (1) (2009) 18–23.

[5] M.M. Shenoy, L.V. Smith, J.T. Axtell, Performance assesment of wood, metal and composite baseball bats, Compos. Struct. 52 (2001) 397–404.
[6] B.J. Maranzano, G. Kaul, B.C. Hancock, Rapid method for measuring the mechanical properties of pharmaceutical compacts, Powder Technol. 236 (2013) 205–210.
[7] G. van Rossum, F.L. Drake, http://docs.python.org/ref/ref.htmlPython reference manual, python software foundation, http://docs.python.org/ref/ref.htmlURL http://docs.python.org/ref/ref.html 2006–2011.
[8] E. Jones, T. Oliphant, P. Peterson, et al., http://www.scipy.org/Scipy: Open source scientific tools for python, http://www.scipy.org/URL http://www.scipy.org/ 2001–2011.
[9] Y. Tsuji, T. Tanaka, T. Ishida, Lagrangian numerical simulation of plug flow of cohesionless particles in a horizontal pipe, Powder Technol. 71 (3) (1992) 239–250.
[10] D. Antypov, J.A. Elliott, On an analytical solution for the damped hertzian spring, Europhys. Lett. 94 (50,004) (2011) 1–6.